PLANT IMMUNITY

Activation of a helper NLR by plant and bacterial TIR immune signaling

Hua Yu[1,2]†, Weiying Xu[1,2]†, Sisi Chen[1,2]†, Xiaoxian Wu[1], Weiwei Rao[1], Xiaoxiao Liu[1], Xiaoyan Xu[1], Jingqi Chen[1,2], Marc T. Nishimura[3], Yu Zhang[1], Li Wan[1]*

Plant intracellular nucleotide-binding leucine-rich repeat (NLR) receptors with an N-terminal Toll/interleukin-1 receptor (TIR) domain sense pathogen effectors to initiate immune signaling. TIR domains across different kingdoms have NADase activities and can produce phosphoribosyl adenosine monophosphate/diphosphate (pRib-AMP/ADP) or cyclic ADPR (cADPR) isomers. The lipase-like proteins EDS1 and PAD4 transduce immune signals from sensor TIR-NLRs to a helper NLR called ADR1, which executes immune function. We report the structure and function of an *Arabidopsis* EDS1-PAD4-ADR1 (EPA) heterotrimer in complex with pRib-AMP/ADP activated by plant or bacterial TIR signaling. 2′cADPR can be hydrolyzed into pRib-AMP and thus activate EPA signaling. Bacterial TIR domains producing 2′cADPR also activate EPA function. Our findings suggest that 2′cADPR may be the storage form of the unstable signaling molecule pRib-AMP.

Plants express cell-surface pattern recognition receptors (PRRs) and intracellular nucleotide-binding leucine-rich repeat (NLR) receptors, which activate pathogen associated molecular pattern-triggered immunity (PTI) and effector-triggered immunity (ETI), respectively (*1*, *2*). Upon sensing pathogen effectors, plant TIR-NLRs (TNLs) function as NADases and produce small signaling molecules (*3*, *4*). Downstream of sensor TNLs, two helper NLRs, Activated Disease Resistance 1 (ADR1) and N Required Gene 1 (NRG1), execute immune functions (*5*). ADR1 and NRG1 carry an Resistance to Powdery Mildew 8 (RPW8)–like coiled coil (CC^R) domain at their N termini and are thus known as CC^R-NLRs (RNLs) (*6*, *7*). Three lipase-like proteins, Enhanced Disease Susceptibility 1 (EDS1), Senescence-Associated Gene 101 (SAG101), and Phytoalexin Deficient 4 (PAD4), function in the TNL pathway by transducing immune signals from sensor TNLs to helper RNLs (*8*, *9*).

Effector-activated TNLs form tetrameric resistosomes with enzymatic activities and produce small signaling molecules including ADP-ribosylated ATP(ADPr-ATP), ADPr-ADPR (di-ADPR), and phosphoribosyl adenosine monophosphate/diphosphate (pRib-AMP/ADP) (*10*–*13*). ADPr-ATP and di-ADPR bind to the EDS1-SAG101 heterodimer and induce the interaction between EDS1-SAG101 and NRG1 to trigger cell death in *Arabidopsis* (*11*, *14*, *15*). pRib-AMP/ADP bind to the EDS1-PAD4 heterodimer and induce the association between EDS1-PAD4 and ADR1 to activate defense and resistance in *Arabidopsis* (*10*, *16*). TNL activation ultimately causes oligomerization of NRG1 and self-association of ADR1 (*16*–*18*). Auto-active NRG1 and ADR1 have been shown to oligomerize and function as calcium channels, similar to effector activated CC-NLR (CNL) immune receptors (*19*–*21*).

Plant and bacterial TIR domains have NAD^+-hydrolyzing and ADPR cyclization activities to produce ADPR, cADPR, and cADPR isomers (*4*, *22*–*25*). Two reported cADPR isomer structures are 2′cADPR and 3′cADPR (*22*). The TIR-containing immune receptor ThsB from the bacterial Thoeris system produces 3′cADPR as a signaling molecule to activate antiviral immunity (*22*, *23*). The TIR-containing effector HopAM1 of the plant pathogen *Pseudomonas syringae* pv. *tomato* DC3000 also generates 3′cADPR, and the production of 3′cADPR correlates with plant immunity suppression through an uncharacterized mechanism (*22*, *26*). 2′cADPR is produced by the TIR-containing effector HopBY of a *P. syringae* strain, indicating a potential function in plant immunity suppression (*27*). However, plant TIR-only proteins and TNLs produce 2′cADPR, which suggests a potential immune activation role of 2′cADPR (*4*, *23*).

We report structures of the *Arabidopsis* EPA heterotrimer induced by the TIR domain of *Arabidopsis* TNL RPS4 and the bacterial TIR-containing effector HopBY. Hydrolytic conversion of 2′cADPR into pRib-AMP activates EPA signaling, which indicates the positive role of 2′cADPR in regulating plant immunity and likely explains the immune cross-talk between plant TIR domains and bacterial TIR domains producing 2′cADPR.

[1]Key Laboratory of Plant Design, CAS Center for Excellence in Molecular Plant Sciences, Institute of Plant Physiology and Ecology, Chinese Academy of Sciences, Shanghai 200032, China. [2]University of Chinese Academy of Sciences, Beijing 100049, China. [3]Department of Biology, Colorado State University, Fort Collins, CO 80523, USA.
*Corresponding author. Email: lwan@cemps.ac.cn
†These authors contributed equally to this work.

Results

Cryo–electron microscopy structure of the EDS1-PAD4-ADR1$^{WHD\text{-}LRR}$ heterotrimer activated by a plant TIR

Activation of TIR signaling has been shown to induce the association between EDS1-PAD4 and ADR1 in insect cells and in planta (*10*, *16*). The nucleotide-binding (NB) domain of NLRs can be divided into three subdomains, the NB domain, helical domain 1 (HD1), and the winged-helix domain (WHD) (*28*). An N-terminally truncated *Arabidopsis* ADR1 named ADR1(1C) containing only the WHD and LRR domains was designed based on the domain architecture of the naturally occurring RNL NRG1C, which negatively regulates EDS1-SAG101-NRG1 signaling (*16*, *29*). ADR1(1C) associates with the EDS1-PAD4 heterodimer in vivo and likely acts as a dominant negative to interfere with EPA signaling (*16*). Full-length ADR1 protein was not expressed as a soluble protein in our insect cell expression system. Considering that the WHD and LRR domains of ADR1 are sufficient for interacting with EDS1-PAD4, we co-expressed ADR1$^{WHD\text{-}LRR}$ (residues 374 to 787), EDS1, PAD4, and the TIR domain (residues 1 to 236) of *Arabidopsis* TNL RPS4 (hereafter RPS4^{TIR}) in insect cells (Fig. 1A) (*10*). The purified protein complex of EDS1-PAD4-ADR1$^{WHD\text{-}LRR}$ behaved as a stable heterotrimer (fig. S1) and was subjected to cryo–electron microscopy (cryo-EM) analyses. After three-dimensional (3D) classification, a subset of 150,167 particles was used for image reconstruction, generating a map with a global resolution of 3.0 Å (fig. S2 and table S1).

The cryo-EM density map showed unambiguous signals for the full-length EDS1-PAD4 heterodimer and ADR1$^{WHD\text{-}LRR}$ (Fig. 1, A and B). A pRib-ADP molecule was identified between EDS1 and PAD4 (Fig. 1C and fig. S3A). The WHD and LRR domains of ADR1 in the heterotrimer structure were positioned in a similar way to CNLs, such as the inactive *Arabidopsis* ZAR1 (PDB: 6J5W), active ZAR1 (PDB: 6J6I), and active wheat Sr35 (PDB: 7XC2) (fig. S3B), suggesting that the WHD-LRR maintains a rigid NLR structural unit. EDS1-PAD4 in the heterotrimer superimposed well with the previously reported structure of pRib-ADP-bound EDS1-PAD4 heterodimer (PDB: 7XEY) [root mean square deviation (RMSD) 1.06 Å for all Cα atoms] (*10*) (fig. S3C). Therefore, the EDS1-PAD4-ADR1$^{WHD\text{-}LRR}$ heterotrimer structure represents a state in which the complex has been activated by TIR signaling.

The interactions between EDS1-PAD4 and ADR1 are critical for activation of ADR1

Superimposing the ligand-free EDS1-PAD4 structure (PDB: 7XDD) onto the ligand-bound EDS1-PAD4 in the heterotrimer context revealed incompatibility between the EP domains of the ligand-free EDS1-PAD4 and the C-terminal

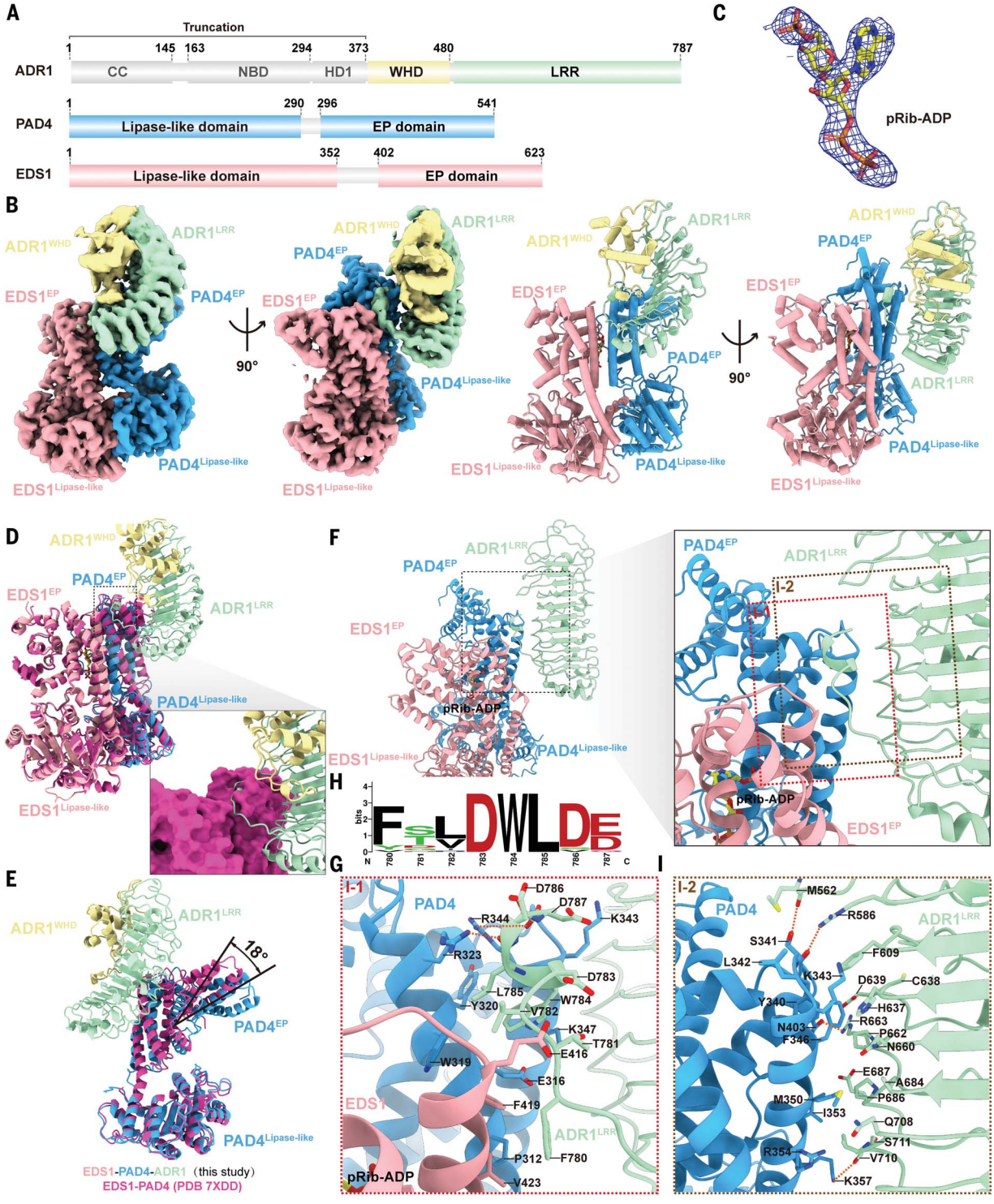

Fig. 1. Cryo-EM structure of the EDS1-PAD4-ADR1$^{WHD-LRR}$ heterotrimer activated by the plant RPS4^{TIR}. (**A**) Schematic representation of *Arabidopsis* EDS1, PAD4, and ADR1 domain architecture. The truncated domains of ADR1 are displayed in gray. (**B**) Overall structure of *Arabidopsis* EDS1-PAD4-ADR1$^{WHD-LRR}$ complexed with pRib-ADP. The cryo-EM map and structure model of EDS1-PAD4-ADR1$^{WHD-LRR}$ are presented in two different orientations. (**C**) Cryo-EM density map of pRib-ADP in the structure of EDS1-PAD4-ADR1$^{WHD-LRR}$. (**D** and **E**) Superimposition of the inactive ligand-free EDS1-PAD4 structure (PDB: 7XDD; magenta) onto EDS1-PAD4 in the heterotrimer context. (D) The incompatibility between ADR1^{LRR} and PAD4 is shown within a black dashed box. The magnified ligand-free EDS1-PAD4 is displayed as a surface representation. (E) For better clarity, EDS1 is omitted in this panel. (**F**) Overall structure of EDS1-PAD4-ADR1$^{WHD-LRR}$ highlighting I-1 and I-2 indicated by red and blue dashed boxes, respectively. (**G**) Cartoon representation of the interaction details in I-1. The interface residues are highlighted in stick representation. H-bonds are shown in red dashed lines. (**H**) Sequence logos showing the conservation of the residues at C terminus of ADR1s by the WebLogo server (*39*). (**I**) Cartoon representation of the interaction details in I-2.

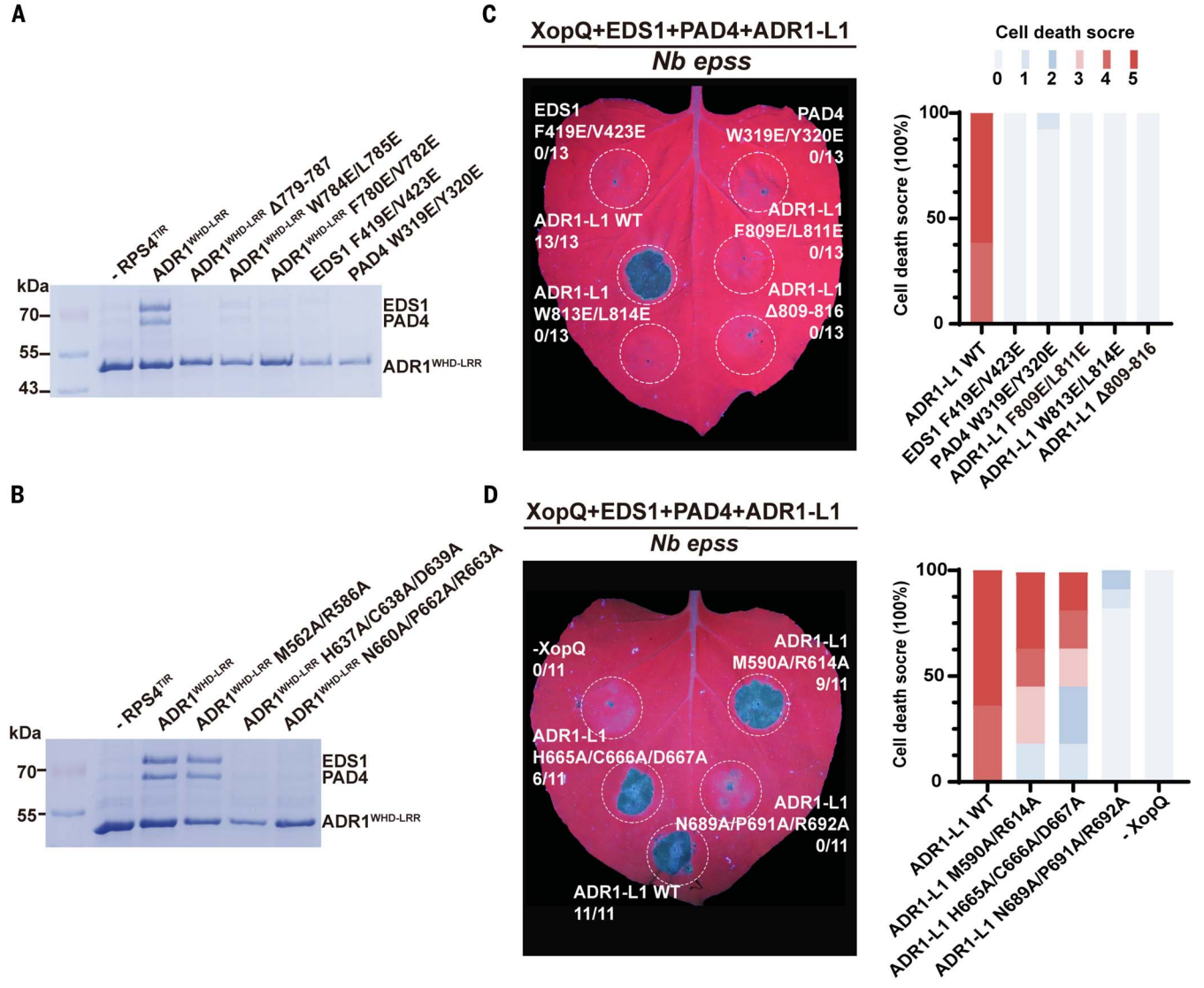

Fig. 2. The interactions between EDS1-PAD4 and ADR1 are critical for function. (**A** and **B**) Mutations in I-1 (A) and I-2 (B) affect the ability of $ADR1^{WHD\text{-}LRR}$ to pull down the EDS1-PAD4 heterodimer. Flag resins were used to pull down Flag-tagged $ADR1^{WHD\text{-}LRR}$ and its interactors. The pull-down assays were repeated three times with similar results. (**C** and **D**) Mutations of specific residues in I-1 (C) and I-2 (D) of ADR1-L1 affect the cell death phenotype when coexpressed with effector XopQ and *Arabidopsis* EDS1 and PAD4 in *Nb epss*. *Agrobacteria* carrying indicated variants were infiltrated into *Nb epss* leaves. The images were taken at 48 hours post infiltration (hpi, hereafter) under UV light. White dotted circles indicate infiltrated areas. The corresponding percentage representation of cell death scores is shown on the right.

helix of ADR1. The interaction cleft at the interface of the ligand-free EDS1-PAD4 heterodimer is not available to accommodate the C-terminal helix of ADR1 (Fig. 1D). These observations explain how the interaction arises from ligand binding, which induces rotation of the PAD4 EP domain by about 18° to create the interaction cleft at the interface of EDS1 and PAD4 (*10*) (Fig. 1E). In the heterotrimer, two major interaction interfaces were observed between EDS1-PAD4 and ADR1. Interaction interface 1 (I-1) mainly involves the loop-helix region at the C terminus of ADR1 and the EP domains of EDS1 and PAD4 with buried surface areas of 585.3 $Å^2$ (Fig. 1F). In I-1, extensive hydrophobic interactions occur involving the residues $F780^{ADR1}$, $V782^{ADR1}$, $W784^{ADR1}$, $L785^{ADR1}$, $W319^{PAD4}$, $Y320^{PAD4}$, $F419^{EDS1}$, and $V423^{EDS1}$ (Fig. 1G and fig. S4A). In addition, $L785^{ADR1}$ and $D787^{ADR1}$ make H-bond interactions with $R323^{PAD4}$ and $R344^{PAD4}$ (Fig. 1G and fig. S4A). Relevant interacting residues of ADR1 fall in a conserved motif, "FTVDWLDD," at the C terminus of ADR1s from different plant species (Fig. 1H and fig. S5A). Relevant interacting residues from EDS1 and PAD4 are also conserved in different plant species (fig. S5B). A similar motif of "YNLDWLVD" was identified at the C terminus of rice ADR1 (fig. S5A), and highly similar interactions were observed in the reported rice EPA structure (*30*). Based on these observations, we generated specific ADR1 mutants in I-1, including deletion of the "FTVDWLDD" motif and neighboring residues (hereafter $\Delta^{779\text{-}787}$), F780E/V782E and W784E/L785E, in addition to EDS1 F419E/V423E, and PAD4 W319E/Y320E. Interaction interface-2 (I-2) involves polar and hydrophobic interactions by the PAD4 EP domain (residues Y340, S341, K343, F346, I353, K357, and N403) and the ADR1 LRR domain (M562, R586, H637, C638, D639, N660, P662, R663, and V710) with buried surface areas of 593.3 $Å^2$ (Fig. 1, F and I, and fig. S4B). We also generated one double mutant M562A/R586A and two triple mutants,

including H637A/C638A/D639A and N660A/P662A/R663A of ADR1, to investigate the functional relevance of I-2.

Mutants in I-1 and I-2 (except M562A/R586A of ADR1) attenuated the ability of ADR1$^{WHD-LRR}$ to pull down the EDS1-PAD4 heterodimer when coexpressed with RPS4^{TIR} in insect cells (Fig. 2, A and B, and fig. S6, A and B). Coexpression of *Arabidopsis* EDS1, SAG101, and NRG1 can complement *Nicotiana benthamiana* (*Nb*) *epss* (*eds1a*, *pad4*, *sag101a*, *sag101b*) to restore the cell death phenotype upon activation by the effector XopQ, which is recognized by an endogenous TNL Roq1 in *Nb* (*14*). In *Arabidopsis*, there are three ADR1 paralogs with redundant functions: ADR1, ADR1-L1, and ADR1-L2 (*31*). Given that ADR1, but not ADR1-L1, is autoactive and causes cell death by itself when transiently overexpressed in *Nb*, we tested if *Arabidopsis* EDS1, PAD4, and ADR1-L1 could complement *Nb epss* to restore the EPA signaling module. Coexpression of *Arabidopsis* EDS1, PAD4, and ADR1-L1 triggered XopQ-dependent cell death, and all corresponding mutants in I-1 abolished the cell death phenotype of XopQ-activated ADR1-L1 when coexpressed with EDS1 and PAD4 in *Nb epss* (Fig. 2C and fig. S6, C and D). The corresponding mutants in I-2 (except M590A/R614A) abolished or attenuated the cell death phenotype of XopQ-activated ADR1-L1 when coexpressed with EDS1 and PAD4 in *Nb epss* (Fig. 2D and fig. S6, D and E). Therefore, I-1 and I-2 collectively mediate the interactions between ADR1 and EDS1-PAD4 and thus are critical for TNL function.

Bacterial TIR domains producing 2′cADPR induce EPA heterotrimerization and activate function

A plant TIR-only protein from *Brachypodium distachyon* (hereafter BdTIR) has been shown to produce 3′cADPR as a minor product to cross-activate the prokaryotic Thoeris immune system (*23*, *32*). To investigate whether bacterial TIR domains cross-activate plant EDS1 pathways, we coexpressed components of EDS1-PAD4-ADR1$^{WHD-LRR}$ or EDS1-SAG101-NRG1A L134E with bacterial TIR-containing proteins including HopBY, HopAM1, and AbTir from *Acinetobacter baumannii* and AaTir from *Aquimarina amphilecti* in insect cells (*22*). The 2′cADPR-producing bacterial TIR-containing protein HopBY and the core TIR domain of AbTir (hereafter AbTir^{TIR}, residues 134 to 269) induced the heterotrimer formation of EDS1-PAD4-ADR1$^{WHD-LRR}$ (Fig. 3A and fig. S7A). The 3′cADPR-producing bacterial TIR-containing protein HopAM1 or the core TIR domain of AaTir (hereafter AaTir^{TIR}, residues 2 to144) did not induce the heterotrimer formation of EDS1-PAD4-ADR1$^{WHD-LRR}$ (Fig. 3A and fig. S7A). All TIR domains that function as active NADases contain an absolutely conserved catalytic glutamate (*4*, *24*). The catalytically dead mutants HopBY E305A and AbTir^{TIR} E208A failed to induce the heterotrimer formation of EDS1-PAD4-ADR1$^{WHD-LRR}$ (Fig. 3A and fig. S7A). The NRG1A L134E mutant has been well demonstrated to abolish the oligomerization of either effector-induced NRG1A or activation mimic NRG1A D485V allele (*18*, *20*). Coexpression of EDS1, SAG101, and RPS4-TIR with NRG1A L134E, but not NRG1A wild type, in insect cells led to successful purification of the heterotrimer protein complex. Neither bacterial TIR was able to induce the heterotrimer formation of EDS1-SAG101-NRG1A L134E (Fig. 3B and fig. S7B), whereas plant RPS4^{TIR} was able to induce the heterotrimer formation of both EDS1-PAD4-ADR1$^{WHD-LRR}$ and EDS1-SAG101-NRG1 L134E (Fig. 3, A and B). These results demonstrate that 2′cADPR-producing bacterial TIRs specifically induce EDS1-PAD4-ADR1$^{WHD-LRR}$ heterotrimer formation.

We further investigated the abilities of bacterial TIR proteins to trigger cell death through the EDS1-PAD4-ADR1-L1 module or the EDS1-SAG101-NRG1A module upon coexpression in *Nb epss*. Consistent with their specific abilities to induce the heterotrimer formation of EDS1-PAD4-ADR1$^{WHD-LRR}$ in insect cells, HopBY and AbTir^{TIR} triggered cell death through the EDS1-PAD4-ADR1-L1 module, but not the EDS1-SAG101-NRG1A module (Fig. 3C and figs. S7C and S8). Both HopBY E305A and AbTir^{TIR} E208A failed to cause cell death (Fig. 3D and fig. S7D). AbTir^{TIR} W204A, a previously characterized mutant with compromised ability in the production of 2′cADPR, triggered attenuated cell death (Fig. 3D and fig. S7D). Neither the 3′cADPR-producing HopAM1 nor AaTir^{TIR} triggered cell death through either module, whereas plant RPS4^{TIR} caused cell death through both the EDS1-PAD4-ADR1-L1 and EDS1-SAG101-NRG1A modules (fig. S9). Consistent with their cell death function, HopBY and AbTir^{TIR} triggered oligomerization of ADR1-L1 dependent on their catalytic activities when coexpressed with EDS1 and PAD4 in *Nb epss*, as did RPS4^{TIR} in Blue Native PAGE (BN-PAGE) assays, but not HopAM1 or AaTir^{TIR} (Fig. 3E). The accumulation of 2′cADPR or 3′cADPR upon expression of the bacterial TIRs and RPS4^{TIR} in *Nb epss* was quantified by mass spectrometry. Both HopBY and AbTir^{TIR}, but not HopBY E305A or AbTir^{TIR} E208A, accumulated 2′cADPR, whereas AbTir^{TIR} W204A produced about two times more 2′cADPR than AbTir^{TIR} E208A (Fig. 3F). RPS4^{TIR} accumulated 2′cADPR about 6 and 2.5% of the yield of HopBY and AbTir^{TIR}, respectively (Fig. 3F). Both HopAM1 and AaTir^{TIR}, but not the catalytically dead HopAM1 E191Q or AaTir^{TIR} E83Q, accumulated 3′cADPR (Fig. 3G). Therefore, bacterial 2′cADPR-producing TIR proteins specifically activate plant EDS1-PAD4-ADR1 immune signaling, and the activation correlates with their capacity to produce 2′cADPR.

Bacterial TIR domains that produce 2′cADPR use pRib-AMP to activate the EPA complex

To further investigate the signaling molecules produced by bacterial TIRs, we purified and denatured the EDS1-PAD4-ADR1$^{WHD-LRR}$ heterotrimer proteins induced by RPS4^{TIR}, HopBY, or AbTir^{TIR} and analyzed them by mass spectrometry. 2′cADPR was not detected in any of the TIR-induced heterotrimer proteins (Fig. 4A). The signaling molecule pRib-AMP was detected in all three cases (Fig. 4B and fig. S10A), whereas pRib-ADP was also detected in the RPS4^{TIR}- and HopBY-induced heterotrimers (fig. S10B). We then solved the cryo-EM structure of the HopBY-induced EDS1-PAD4-ADR1$^{WHD-LRR}$ heterotrimer at a global resolution of 3.3 Å (fig. S11 and table S1). The structures of HopBY- and RPS4^{TIR}-induced EDS1-PAD4-ADR1$^{WHD-LRR}$ heterotrimers superimposed well (RMSD 0.64 Å for all Cα atoms), indicating similar activation and assembly mechanisms of the EDS1-PAD4-ADR1$^{WHD-LRR}$ complex by plant and bacterial TIR domains (Fig. 4C and fig. S12, A and B). A pRib-AMP molecule was identified between EDS1 and PAD4 in the HopBY-induced EDS1-PAD4-ADR1$^{WHD-LRR}$ heterotrimer structure, whereas a pRib-ADP molecule was identified in the RPS4^{TIR}-induced EDS1-PAD4-ADR1$^{WHD-LRR}$ heterotrimer structure (Fig. 4D and fig. S12C). Therefore, both plant and bacterial TIRs use pRib-AMP/ADP as signaling molecules to activate plant EDS1-PAD4-ADR1 signaling.

Hydrolytic conversion of 2′cADPR into pRib-AMP induces EPA-dependent defense signaling

Given that 2′cADPR and pRib-AMP are structurally related molecules and hydrolysis of 2′cADPR through the pyrophosphate bond gives rise to pRib-AMP (Fig. 5A), we tested the conversion of 2′cADPR into pRib-AMP. Incubation of 2′cADPR with a protein extract of *Arabidopsis* Col-0 leaves led to the detection of pRib-AMP after protection with purified EDS1-PAD4 heterodimer protein, supporting the conversion of 2′cADPR to pRib-AMP (Fig. 5, B and C, and fig. S13). Detection of pRib-AMP in these cases requires protection by purified ligand-free EDS1-PAD4 heterodimer proteins, as previously reported (*10*, *11*), further indicating the instability of pRib-AMP. To further investigate whether 2′cADPR directly activates plant immunity, purified chemicals of 2′cADPR and 3′cADPR were infiltrated into the leaves of Col-0, *eds1-12*, *sag101*, *pad4-1*, *nrg1a nrg1b*, and *adr1/adr1-l1/adr1-l2* (*adr1 triple*) and quantitative polymerase chain reaction (q-PCR) was performed to analyze defense gene expression. 2′cADPR but not 3′cADPR caused strong induction of *Pathogenesis-Related Protein 1* (*PR1*) (Fig. 5D). 2′cADPR also induced the expression of defense marker gene FLG22-induced receptor-like kinase 1 (FRK1) and salicylic acid and systemic acquired resistance–related genes at

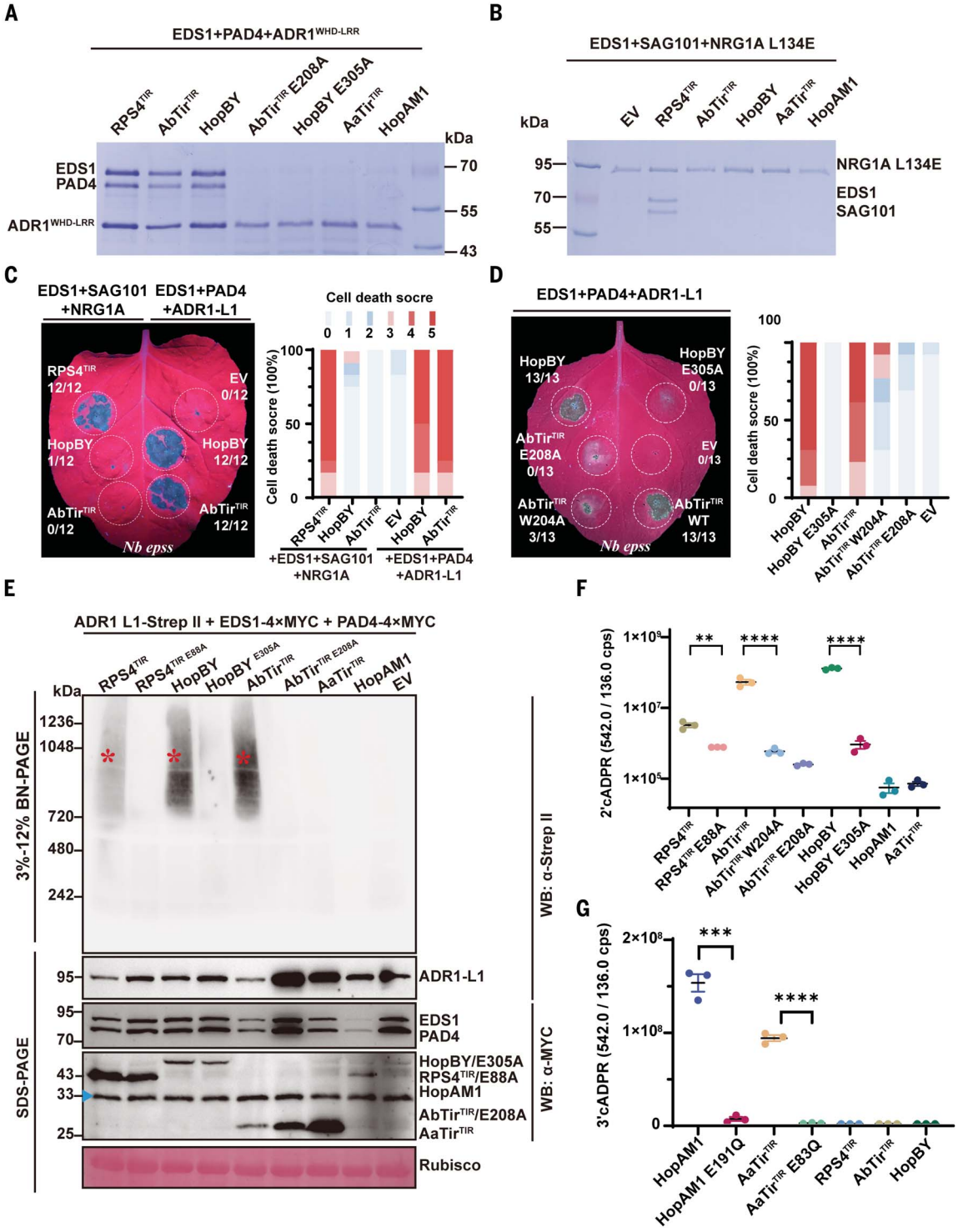

Fig. 3. Bacterial TIRs producing 2′cADPR induce the EPA complex and activate function. (**A**) HopBY, AbTir^{TIR}, HopAM1, or AaTir^{TIR} was coexpressed with ADR1$^{WHD-LRR}$ and EDS-PAD4 in insect cells. Flag resins were used to pull down Flag-tagged ADR1$^{WHD-LRR}$ and its interactors. (**B**) HopBY, HopAM1, AbTir^{TIR}, or AaTir^{TIR} was coexpressed with NRG1A^{L134E} and EDS1-SAG101 in insect cells. Flag resins were used to pull down Flag-tagged NRG1A^{L134E} and its interactors. The pull-down assays were repeated three times with similar results. (**C** and **D**) Cell death phenotypes of HopBY and AbTir^{TIR} when coexpressed with the EDS1-PAD4-ADR1-L1 module or the EDS1-SAG101-NRG1A module in *Nb epss*. White dotted circles indicate *Agrobacteria*-infiltrated areas. The images were taken at 40 and 48 hpi for (C) and (D), respectively. The corresponding percentage representation of cell death scores is shown on the right. (**E**) BN-PAGE assays showing the oligomerization of ADR1-L1 triggered by plant or bacterial TIRs when coexpressed with EDS1-PAD4 in *Nb epss*. BN-PAGE assays were repeated three times with similar results. Red asterisks indicate the oligomerized ADR1-L1, and a blue triangle points to a contaminant protein band. (**F** and **G**) The accumulation of 2′cADPR (F) and 3′ cADPR (G) upon expression of bacterial TIR-containing proteins and RPS4^{TIR} in *Nb epss* leaves. Data are shown as mean ± SEM; $n = 3$ biological repeats. Samples were collected at 48 hpi, and metabolites were analyzed using liquid chromatography–mass spectrometry (LC-MS). Asterisks indicate significant differences analyzed by two-tailed t test (**$P \leq 0.01$, ***$P \leq 0.001$, ****$P \leq 0.0001$).

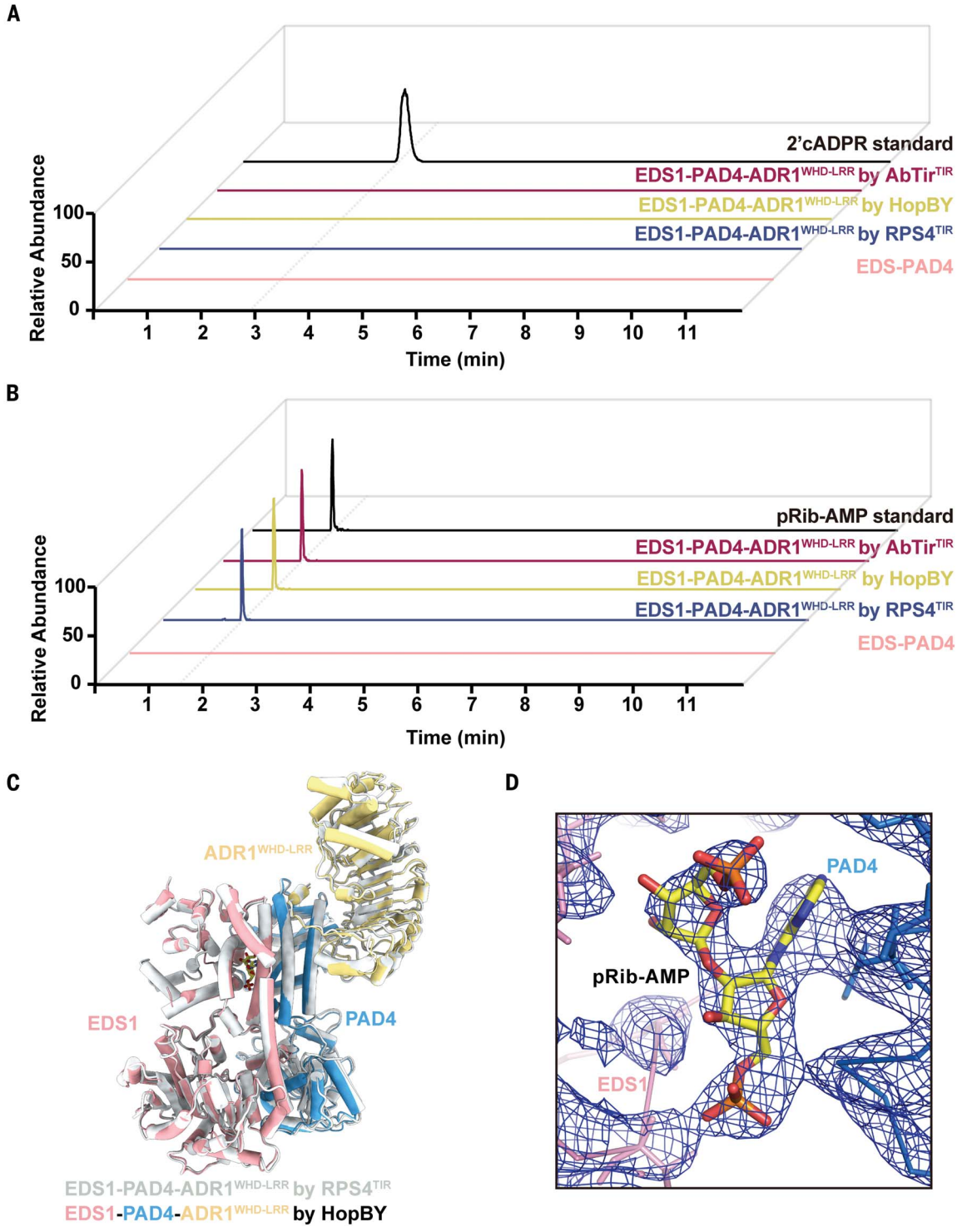

Fig. 4. HopBY and AbTir^{TIR} use pRib-AMP as the signaling molecule to induce EDS1-PAD4-ADR1$^{WHD-LRR}$ heterotrimer formation. (**A** and **B**) LC-MS traces of 2′cADPR (A) and pRib-AMP (B) from EDS1-PAD4-ADR1$^{WHD-LRR}$ heterotrimer proteins induced by HopBY, AbTir^{TIR}, or RPS4^{TIR} relative to their standards. The complex proteins were induced, expressed, and purified from insect cells. Bound small molecules were extracted by denaturing the complex proteins with 80% methanol (v/v) and then subjected to LC-MS. (**C**) Superimposition of the RPS4^{TIR} and HopBY induced EDS1-PAD4-ADR1$^{WHD-LRR}$ heterotrimer structures. (**D**) Cryo-EM density map of pRib-AMP in the structure of EDS1-PAD4-ADR1$^{WHD-LRR}$ induced by HopBY.

6 hours after infiltration (fig. S14). The induction of these defense genes was dependent on the EDS1-PAD4-ADR1 module, but not on SAG101 or NRG1 (Fig. 5E and fig. S14). To further investigate how many genes were induced in an EPA-dependent manner, we performed RNA-sequencing (RNA-seq) experiments on 2′cADPR-treated Col-0 and *pad4-1* leaf samples (fig. S15A). RNA-seq analyses revealed 2593 up-regulated genes and 3453 down-regulated genes in Col-0 (Fig. 5F and fig. S15, B and C). These differentially regulated genes were almost not responsive in *pad4-1*. Gene ontology (GO) analyses revealed that the up-regulated genes were mainly enriched in various defense pathways, and the down-regulated genes were mainly enriched in photosynthesis and auxin signaling pathways (fig. S15, D and E). These results are consistent with previous findings on photosynthetic inhibition in ETI and the concept of defense-growth trade-offs (*33*, *34*).

Consistent with activation of EPA signaling, infiltration of 2′cADPR into Col-0 did not cause cell death but triggered resistance against

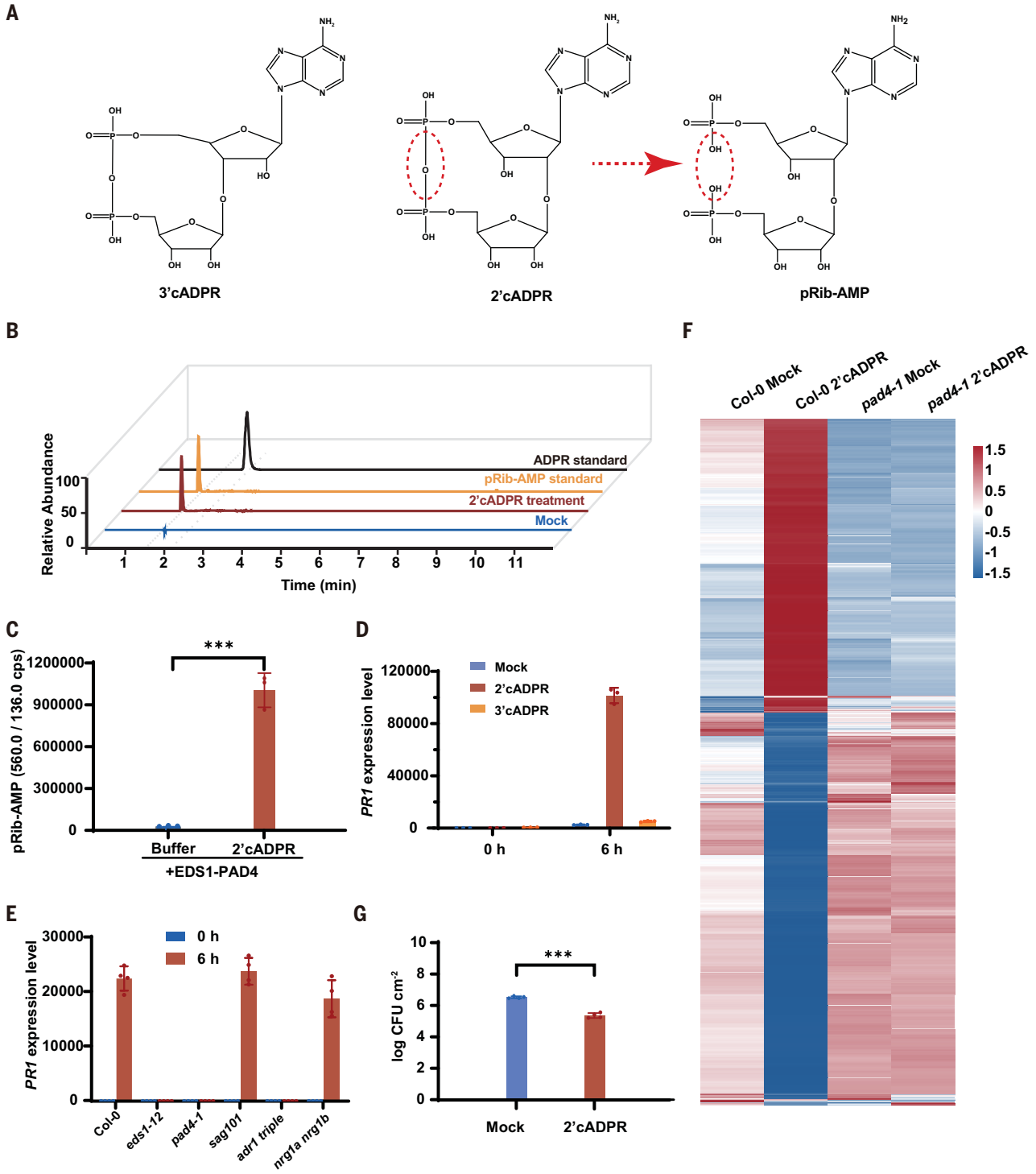

Fig. 5. Hydrolytic conversion of 2′cADPR into pRib-AMP induces EDS1-PAD4-ADR1 dependent defense signaling. (**A**) Chemical structures of 3′cADPR, 2′cADPR, and pRib-AMP. Hydrolysis of the pyrophosphate bond of 2′cADPR in the red dashed circle gives rise to pRib-AMP. (**B**) Conversion of 2′cADPR into pRib-AMP in vivo. LC-MS traces of pRib-AMP from 2′cADPR relative to ADPR and pRib-AMP standards. The leaf lysate of Col-0 was divided into two batches, with one batch treated with 2′cADPR and the other mock treated for 48 hours at 4°C. Purified ligand-free EDS1-PAD4 heterodimer proteins were used to capture pRib-AMP and then denatured with 80% methanol (v/v). (**C**) The samples were subjected to LC-MS analyses, and detection of pRib-AMP was quantified. Data are shown as mean ± SD; $n = 3$ technical repeats. Asterisks indicate significant differences analyzed by two-tailed t test (***$P \leq 0.001$). (**D**) The expression of *PR1* upon treatment of Col-0 with 2′cADPR or 3′cADPR analyzed by q-PCR. Data are shown as mean ± SD; $n = 3$ biological repeats. (**E**) Expression of *PR1* upon treatment of Col-0, *eds1-12*, *pad4-1*, *sag101*, *adr1 triple*, and *nrg1a nrg1b* with 2′cADPR and analysis by q-PCR. Data are shown as mean ± SD; $n = 4$ biological repeats. (**F**), Hierarchical clustering of total differentially expressed genes in 2′cADPR or mock-treated leaves of Col-0 and *pad4-1* in RNA-seq experiments. (**G**) Growth of *P. syringae* pv. *tomato DC3000* (D36E) in *Arabidopsis* leaves infiltrated with 50 μM 2′cADPR at 4 dpi. Bacteria at optical density at 600 nm (OD_{600nm}) of 0.01 treated with 50 μM 2′cADPR or mock treated were infiltrated, and populations were determined as log_{10}-transformed colony-forming unit values. Asterisks indicate significant differences analyzed by two-tailed t test (***$P \leq 0.001$). Data are shown as mean ± SD; $n = 4$ biological repeats.

Pseudomonas syringae pv. *tomato DC3000* (D36E), a derivative of the strain that lacks all endogenous effectors (Fig. 5G and fig. S16A). To further validate this, we infiltrated 2′cADPR into *Nb epss* leaves expressing EDS1/PAD4/ADR-L1 and observed cell death phenotype (fig. S16, B and C). Hence 2′cADPR activates EDS1-PAD4-ADR1 immune signaling likely via hydrolytic conversion into pRib-AMP.

Discussion

Activation of TIR signaling leads to heterotrimer formation of EDS1-PAD4-ADR1 and EDS1-SAG101-NRG1, and ultimately oligomerization of NRG1 and ADR1 (Fig. 4E) (*10*, *11*, *15*–*18*). The relationship between EDS1-PAD4-ADR1 heterotrimer formation and ADR1 oligomerization remains to be resolved. The structures of oligomeric ADR1 and NRG1 would enable understanding of their calcium channel activities at the plasma membrane (*18*, *20*). The localization of the EDS1-PAD4-ADR1 heterotrimer requires further investigation to establish whether it is in the nucleus similarly to the EDS1-SAG101-NRG1 heterotrimer (*17*). The cryo-EM structures of *Arabidopsis* and rice EDS1-PAD4-ADR1 heterotrimers bound with pRib-AMP/ADP highlight the biological function of TIR-produced signaling molecules in modifying host EDS1-PAD4 to activate the helper RNL ADR1 in both dicots and monocots (*30*). Upon binding of ADPr-ATP or di-ADPR, EDS1-SAG101 likely uses similar mechanisms to activate NRG1 (*10*, *11*, *16*).

In the two interaction interfaces, I-1 mainly involves some conserved residues in the loop-helix region at the C terminus of ADR1 and the EP domains PAD4 and EDS1, which likely defines a common rule for the EDS1-PAD4-ADR1 heterotrimer formation in different plant species. A different motif was identified at the C terminus of NRG1s, which likely accounts for the specific interaction with EDS1-SAG101 in a similar way (fig. S5A). I-2 mainly involves conserved and nonconserved residues in the ADR1 LRR domain and the PAD4 EP domain (fig. S17), which may account for the incompatibility of EDS1, PAD4, and ADR1 from different plant species (*14*, *35*). The key residues in I-2 of ADR1s are mostly different from the corresponding residues in NRG1s (fig. S17), which likely determine the specificity for the EDS1-PAD4-ADR1 interaction. The rigid WHD and LRR domains of ADR1(1C) and NRG1C are sufficient to mediate the interactions with EDS1-SAG101 and EDS1-PAD4, respectively (Fig. 1) (*16*, *29*). These data indicate similar heterotrimer assembly mechanisms between EDS1-PAD4-ADR1 and EDS1-SAG101-NRG1 complexes. The signaling mechanisms that define the specificities of EDS1-PAD4-ADR1 and EDS1-SAG101-NRG1 modules in resistance and cell death in *Arabidopsis*, respectively, await future studies.

The plant BdTIR produces 3′cADPR as a minor product to cross-activate bacterial antiviral immunity (*23*). The 3′cADPR-producing bacterial TIR-containing proteins HopAM1 and AaTir^{TIR} activate neither the EDS1-PAD4-ADR1 nor EDS1-SAG101-NRG1 signaling modules, consistent with the idea that 3′cADPR negatively regulates plant immunity (*22*, *26*). The mechanisms by which 3′cADPR suppresses plant immunity remain unknown. Given that bacterial TIR domains producing 2′cADPR activate EPA signaling, it remains to investigate whether the plant EDS1-PAD4-ADR1 module can be functional in bacteria to confer immunity.

Our work confirms a role for 2′cADPR in positively regulating plant immunity. The TIR-containing effector HopBY from *P. syringae* depends on its catalytic activity and production of 2′cADPR to promote infection of *Arabidopsis* (*27*). HopBY is a strong NADase that causes decline of NAD^+ in host cells compared with the weak NADase activities of plant TIRs (*4*, *27*, *36*). Given the positive role of 2′cADPR in plant EDS1-PAD4-ADR1 immune signaling, it is likely that HopBY-induced decline of host cellular NAD^+ levels plays a role in promoting virulence function, as was proposed previously (*36*).

2′cADPR is a stable molecule that can be readily detected by mass spectrometry, whereas pRib-AMP is highly unstable, and its detection in vivo by mass spectrometry requires protection by purified ligand–free EDS-PAD4 heterodimer proteins (*10*, *11*). Given that the source of pRib-AMP is unclear and the EDS1-PAD4-ADR1 module plays critical roles in both basal immunity and ETI (*37*, *38*), we propose that 2′cADPR functions as a storage form of pRib-AMP to activate EDS1-PAD4-ADR1 signaling. The enzymes involved in the conversion of 2′cADPR into pRib-AMP and how these enzymes regulate plant immunity await future study.

REFERENCES AND NOTES

1. J. D. G. Jones, B. J. Staskawicz, J. L. Dangl, *Cell* **187**, 2095–2116 (2024).
2. J. M. Zhou, Y. Zhang, *Cell* **181**, 978–989 (2020).
3. S. Horsefield *et al*., *Science* **365**, 793–799 (2019).
4. L. Wan *et al*., *Science* **365**, 799–803 (2019).
5. Y. Gong, L. Tian, I. Kontos, J. Li, X. Li, *Curr. Opin. Plant Biol.* **73**, 102354 (2023).
6. L. M. Jubic, S. Saile, O. J. Furzer, F. El Kasmi, J. L. Dangl, *Curr. Opin. Plant Biol.* **50**, 82–94 (2019).
7. X. Liu, L. Wan, *Mol. Plant Pathol.* **23**, 772–780 (2022).
8. F. Locci, J. Wang, J. E. Parker, *Curr. Opin. Plant Biol.* **74**, 102373 (2023).
9. J. A. Dongus, J. E. Parker, *Curr. Opin. Plant Biol.* **62**, 102039 (2021).
10. S. Huang *et al*., *Science* **377**, eabq3297 (2022).
11. A. Jia *et al*., *Science* **377**, eabq8180 (2022).
12. S. Ma *et al*., *Science* **370**, eabe3069 (2020).
13. R. Martin *et al*., *Science* **370**, eabd9993 (2020).
14. D. Lapin *et al*., *Plant Cell* **31**, 2430–2455 (2019).
15. X. Sun *et al*., *Nat. Commun.* **12**, 3335 (2021).
16. Z. Wu, L. Tian, X. Liu, Y. Zhang, X. Li, *Plant Physiol.* **187**, 681–686 (2021).
17. J. M. Feehan *et al*., *Proc. Natl. Acad. Sci. U.S.A.* **120**, e2210406120 (2023).
18. Z. Wang *et al*., *Proc. Natl. Acad. Sci. U.S.A.* **120**, e2222036120 (2023).
19. G. Bi *et al*., *Cell* **184**, 3528–3541.e12 (2021).
20. P. Jacob *et al*., *Science* **373**, 420–425 (2021).
21. A. Förderer *et al*., *Nature* **610**, 532–539 (2022).
22. M. K. Manik *et al*., *Science* **377**, eadc8969 (2022).
23. A. M. Bayless *et al*., *Sci. Adv.* **9**, eade8487 (2023).
24. K. Essuman, J. Milbrandt, J. L. Dangl, M. T. Nishimura, *Science* **377**, eabo0001 (2022).
25. L. Wan, *aBIOTECH* **4**, 172–175 (2023).
26. S. Eastman *et al*., *New Phytol.* **233**, 890–904 (2022).
27. M. T. Hulin, L. Hill, J. D. G. Jones, W. Ma, *Proc. Natl. Acad. Sci. U.S.A.* **120**, e2217114120 (2023).
28. J. Wang *et al*., *Science* **364**, eaav5868 (2019).
29. Z. Wu *et al*., *Plant Cell* **34**, 1621–1640 (2022).
30. Y. Wu *et al*., *Science* **386**, 1405–1412 (2024).
31. V. Bonardi *et al*., *Proc. Natl. Acad. Sci. U.S.A.* **108**, 16463–16468 (2011).
32. G. Ofir *et al*, *Nature* **600**, 116 (2021).
33. J. Su *et al*., *PLOS Biol.* **16**, e2004122 (2018).
34. Z. He, S. Webster, S. Y. He, *Curr. Biol.* **32**, R634–R639 (2022).
35. J. Gantner, J. Ordon, C. Kretschmer, R. Guerois, J. Stuttmann, *Plant Cell* **31**, 2456–2474 (2019).
36. S. C. Ogden, M. T. Nishimura, *Proc. Natl. Acad. Sci. U.S.A.* **120**, e2300970120 (2023).
37. H. Tian *et al*., *Nature* **598**, 500–503 (2021).
38. R. N. Pruitt *et al*., *Nature* **598**, 495–499 (2021).
39. G. E. Crooks, G. Hon, J.-M. Chandonia, S. E. Brenner, *Genome Res.* **14**, 1188–1190 (2004).

ACKNOWLEDGMENTS

We thank Professor Jeffery L. Dangl for critical reading of the manuscript. We thank L. Kong, F. Wang, G. Li, J. Duan at electron microscopy system at the National Facility for Protein Science in Shanghai (NFPS) and the staffs of electron microscopy center at Shuimu Biosciences in Hangzhou for technical support and assistance in cryo-EM data Collection. We thank Z. Zhang and M. Zhang at the core facility of the Center for Excellence in Molecular Plant Sciences (CEMPS) for help with cross-link optimization and cryo-EM sample screening. We thank Y. Y. Gao and L. Y. Jing at CEMPS for the help with LC-MS/MS. **Funding:** L.W. was supported by National Key Research and Development Program of China (2023YFF1000300), Key Laboratory of Plant Design, CAS Center for Excellence in Molecular Plant Sciences, Institute of Plant Physiology and Ecology, Chinese Academy of Sciences, National Natural Science Foundation of China (Project number: 32270304), and Chinese Academy of Sciences Strategic Priority Research Program (Type-B; Project number: XDB27040214). M.T.N was supported by NSF award IOS-1758400. **Author contributions:** Conceptualization: L.W. Methodology: H.Y., W.Y.X., S.S.C., X.X.W., W.W.R., X.X.L., X.Y.X., J.Q.C., M.T.N., Y.Z. and L.W. Investigation: H.Y., W.Y.X., S.S.C., X.X.W., and X.X.L. Funding acquisition: L.W. Supervision: Y.Z. and L.W. Writing: L.W.. **Competing interests:** The authors declare no competing interests. **Data and materials availability:** All data are available in the main text, the supplementary materials or in the Protein Data Bank (PDB) and NCBI files. Atomic coordinates of the two heterotrimers have been deposited in the PDB with accession codes 8ZW9 (RPS4^{TIR} induced EDS1-PAD4-ADR1$^{WHD-LRR}$) and 8ZWA (HopBY induced EDS1-PAD4-ADR1$^{WHD-LRR}$). The raw data of RNA-seq is available through GEO number (GSE277725; https://www.ncbi.nlm.nih.gov/geo/). The total DEGs and GO enrichment are included in Data S1 and S2.

SUPPLEMENTARY MATERIALS

science.org/doi/10.1126/science.adr3150
Materials and Methods
Figs. S1 to S17
Tables S1 to S6
Data S1 and S2
References (*40*–*54*)
MDAR Reproducibility Checklist

Submitted 25 June 2024; accepted 18 October 2024
Published online 7 November 2024
10.1126/science.adr3150